

The Cocoon Nebula and its ionizing star: do stellar and nebular abundances agree?★

J. García-Rojas^{1,2}, S. Simón-Díaz^{1,2} & C. Esteban^{1,2}

¹ Instituto de Astrofísica de Canarias, E-38200 La Laguna, Tenerife, Spain

² Universidad de La Laguna, Dept. Astrofísica, E-38204 La Laguna, Tenerife, Spain.

Submitted 23 July 2014 /Accepted 29 September 2014

ABSTRACT

Context. Main sequence massive stars embedded in an H II region should have the same chemical abundances as the surrounding nebular gas+dust. The Cocoon nebula (IC 5146), a close-by Galactic H II region ionized by a narrow line B0.5 V single star (BD+46 3474), is an ideal target to perform a detailed comparison of nebular and stellar abundances in the same Galactic H II region.

Aims. We investigate the chemical content of oxygen and other elements in the Cocoon nebula from two different points of view: an empirical analysis of the nebular spectrum and a detailed spectroscopic analysis of the associated early B-type star using state-of-the-art stellar atmosphere modeling. By comparing the stellar and nebular abundances, we aim to indirectly address the long-standing problem of the discrepancy found between abundances obtained from collisionally excited lines and optical recombination lines in photoionized nebulae.

Methods. We collect long-slit spatially resolved spectroscopy of the Cocoon nebula and a high resolution optical spectrum of the ionizing star. Standard nebular techniques along with updated atomic data are used to compute the physical conditions and gaseous abundances of O, N and S in 8 apertures extracted across a semidiameter of the nebula. We perform a self-consistent spectroscopic abundance analysis of BD+46 3474 based on the atmosphere code FASTWIND to determine the stellar parameters and Si, O, and N abundances.

Results. The Cocoon nebula and its ionizing star, located at a distance of 800 ± 80 pc, have a very similar chemical composition as the Orion nebula and other B-type stars in the solar vicinity. This result agrees with the high degree of homogeneity of the present-day composition of the solar neighbourhood (up to 1.5 Kpc from the Sun) as derived from the study of the local cold-gas ISM. The comparison of stellar and nebular collisionally excited line abundances in the Cocoon nebula indicates that O and N gas+dust nebular values are in better agreement with stellar ones assuming small temperature fluctuations, of the order of those found in the Orion nebula ($r^2 = 0.022$). For S, the behaviour is somewhat puzzling, reaching to different conclusions depending on the atomic data set used.

Key words. ISM: HII regions – ISM: individual: IC 5146 – ISM: abundances – Stars: early-type – Stars: fundamental parameters – Stars: atmospheres – Stars: individual: BD+46 3474 –

1. Introduction

In nebular astrophysics, the oxygen abundance is the most widely used proxy of metallicity from the Milky Way to far-distant galaxies. A precise knowledge of its abundance, as well as of nitrogen, carbon, α -elements and iron-peak elements and their ratios at different redshifts are crucial to understand the nucleosynthesis processes in the stars and the chemical evolution history of the Universe (Henry et al., 2000; Chiappini et al., 2003; Carigi et al., 2005). Uncertainties in the knowledge of the oxygen abundance (i.e., metallicity) have important implications in several topics of modern Astrophysics such as the luminosity- and mass-metallicity relations for local and high-redshift star-forming galaxies (Tremonti et al., 2004), the calibrations of strong line methods for deriving the abundance scale of extragalactic H II regions and star-forming galaxies at

different redshifts (Peimbert et al., 2007; Peña-Guerrero et al., 2012), or the determination of the primordial helium abundance (Peimbert, 2008).

Ionized nebulae have been always claimed to be the most reliable and straightforward astrophysical objects to determine abundances from close-by to large distances in the Universe. However, they are not free from some difficulties. One of the most longstanding problems is the dichotomy systematically found between the nebular abundances provided by the standard method, based on the analysis of intensity ratios of collisionally excited lines (CELs, which strongly depend on the assumed physical conditions in the nebula) and the abundances given by the faint optical recombination lines (ORLs, which are almost insensitive to the adopted physical conditions).

Already pointed out in the pioneering work by Wyse (1942) in the planetary nebula NGC 7009 more than seventy years ago, the observational evidence of CEL and ORL providing discrepant results has increased significantly in the last decade, both using Galactic H II regions data (Esteban et al., 2005, 2013; García-Rojas & Esteban, 2007, and references therein) and extragalactic H II regions data (Esteban et al., 2002, 2009, 2014; Peimbert, 2003; López-Sánchez et al., 2007; Peña-Guerrero et al., 2012). In particular, these authors have

Send offprint requests to: jogarcia@iac.es

★ Based on observations made with the William Herschel Telescope operated by the Isaac Newton Group and with the Nordic Optical Telescope, operated by the Nordic Optical Telescope Scientific Association. Both telescopes are at the Observatorio del Roque de los Muchachos, La Palma, Spain, of the Instituto de Astrofísica de Canarias.

found that the O^{2+}/H^+ ratio computed from $O\text{II}$ ORLs gives systematically higher values than that obtained from $[O\text{III}]$ CELs by a factor ranging ~ 1.2 – 2.2 . Similar discrepancies have been reported for other ions for which abundances can be determined using both CELs and ORLs: C^{2+} , Ne^{2+} and O^+ (see García-Rojas & Esteban, 2007). The origin of this discrepancy is still unknown and has been subject of debate for many years (see e.g., Tsamis & Péquignot, 2005; Stasińska et al., 2007; Mesa-Delgado et al., 2009b, 2012; Tsamis et al., 2011; Nicholls et al., 2012, 2013; Peimbert & Peimbert, 2013, and references therein for the most recent literature on the subject).

The comparison of nebular abundances with those resulting from the spectroscopic analysis of associated blue massive stars (especially B-type stars in the main sequence and BA Supergiants) is another way to shed some light in the nebular abundance conundrum, particularly, in the absence of nebular ORLs. These stars have been proved to be powerful alternative tools to derive the present-day chemical composition of the interstellar material in the Galactic regions where they are located (similarly to $H\text{II}$ regions). Following this approach, several authors have compared galactic radial abundance gradients obtained from massive stars and $H\text{II}$ regions in nearby spiral galaxies (see Bresolin et al., 2009; Trundle et al., 2002; U et al., 2009, for NGC 300, M 31 and M 33, respectively). When examined together, the outcome of these studies is, however, not completely conclusive. For example, while a total agreement between nebular and stellar abundances is observed in NGC 300 (Bresolin et al., 2009), a remarkable discrepancy is found in M 31 (Trundle et al., 2002). However, the comparison of nebular and stellar abundances in most of these studies are performed in a global way, while there still exists the possibility of local or azimuthal variations of abundances in the studied galaxies hampering a meaningful comparison of abundances. In addition, in several cases, nebular abundances could be only obtained by means of indirect (strong-line) methods and not directly from CELs/ORLs.

To avoid some of these limitations one should concentrate on the study of $H\text{II}$ regions and close-by blue massive stars for which we are confident that have been formed and evolved in the same environment (and hence share the same chemical composition). In addition, a handful set of “technical” conditions must be taken into account: a) the $H\text{II}$ region must be bright enough in order to detect the relatively faint auroral lines to determine T_e and, if possible, a handful set of ORLs, b) the spectra of the stars must show a statistically meaningful set of non-blended metallic lines (stars with spectral types in the range O9-B2 and low projected rotational velocities, $v \sin i < 70 \text{ km s}^{-1}$, are the most suitable targets for this study), c) stars must not belong to binary/multiple systems. There are not many Galactic $H\text{II}$ regions that fulfill all these conditions. Of course, the keystone of all nebular studies, the Orion nebula (M 42), is one of them¹. The comparison of nebular and stellar abundances in the Orion star forming region (as derived from the analysis of the spectra of M 42 and a handful number of early B-type stars in the region²) has been recently reviewed by Simón-Díaz & Stasińska (2011). The main conclusion of this study (which has been actually present in the literature in the last two decades, see e.g., Esteban et al.,

1998, 2004) is that oxygen (gas+dust) nebular abundance based on ORLs agrees much better with the stellar abundances than the one derived from CELs. If a similar thoughtful analysis of a larger sample of targets (including the analysis of other elements and considering different metallicity environments) confirm this result, this will have important implications for several fields of modern Astrophysics and the way the abundance scale in the Universe is defined.

The Cocoon nebula (also known as IC 5146, Caldwell 19 and Sh 2-125) is an emission nebula located in the constellation of Cygnus. Its distance is somewhat uncertain and has been fixed between $950 \pm 80 \text{ pc}$ (Harvey et al., 2008) and $1200 \pm 180 \text{ pc}$ (Herbig & Dahm, 2002). This nebula is an ideal target to perform a detailed comparison of nebular and stellar abundances in the same Galactic region since most of the “technical” conditions quoted above are fulfilled³. The nebula is ionized by a single B0.5 V star –BD46 3474, with low projected rotational velocity– and is bright enough to compute physical conditions and chemical abundances from its nebular emission line spectrum. In addition, the ionization degree of the nebula is low due to the relatively low effective temperature of the central star and then, the most relevant elements are only once ionized and no ionization correction factors (ICF) are needed for determining total abundances of some key-elements.

In this paper we perform a detailed spectroscopic abundance analysis of a set of long-slit spatially resolved intermediate-resolution spectra of the Cocoon nebula and a high-resolution optical spectrum of the ionizing star. The derived nebular CEL and stellar abundances of O, N, and S are hence compared. The paper is structured as follows. The observational data set is presented in Sect. 2. The nebular physical conditions and abundances are determined in Sect. 3. A self-consistent spectroscopic abundance analysis of BD+46 3474 is performed in Sect. 4. The discussion of results and the main conclusions from our study are presented in Sect. 5 and Sect. 6, respectively.

2. The observational data set

2.1. Nebular spectroscopy

A long-slit, intermediate-resolution spectrum of the Cocoon nebula was obtained on 2011 November 23 with the Intermediate dispersion Spectrograph and Imaging System (ISIS) spectrograph attached to the 4.2m William Herschel Telescope (WHT) at Roque de los Muchachos observatory in La Palma (Canary Islands, Spain). The $3.7' \times 1.02''$ slit was located to the north-west of BD+46 3474, ($PA=320^\circ$, see Fig. 1). Two different CCDs were used at the blue and red arms of the spectrograph: an EEV CCD with a configuration 4096×2048 pixels at $13.5 \mu\text{m}$, and a RedPlus CCD with 4096×2048 pixels at $15.0 \mu\text{m}$, respectively. The dichroic prism used to separate the blue and red beams was set at 5300 \AA . The gratings R600B and R316R were used for the blue and red observations, respectively. These gratings give a reciprocal dispersion of 33 \AA mm^{-1} in the blue and 62 \AA mm^{-1} in the red, effective spectral resolutions of 2.2 and 3.56 \AA and the spatial scales are $0.20'' \text{ pixel}^{-1}$ and $0.22'' \text{ pixel}^{-1}$, respectively. We used two different grating angles in order to cover all the optical wavelength range: a) blue spectra centered at 4298 \AA and red one centered at 6147 \AA , and b) blue spectra centered at 4298 \AA and red one centered at 8148 \AA . The blue spectra cover an unvignetted range from $\lambda\lambda 3600$ to 5100 \AA

¹ Among the few others we can cite M 16 (Eagle nebula), NGC3372 (Carina nebula), or IC5146 (Cocoon nebula, studied in this paper)

² The nebular abundance analysis was performed by Esteban et al. (2004), and revisited by Simón-Díaz & Stasińska (2011); the stellar abundance analysis was performed by Simón-Díaz (2010) and Nieva & Simón-Díaz (2011).

³ We do not detect ORLs in the spectrum of the Cocoon nebula, but the discussion can be done in other terms (see Sect. 5).

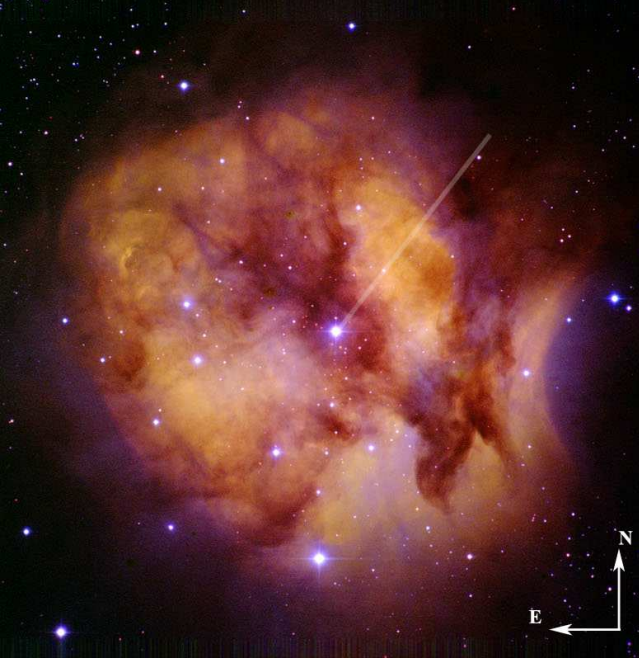


Fig. 1. Color composite (RGB) image of the Cocoon Nebula obtained from a combination of wide and narrow band images taken with the Wide Field Camera (WFC) at the 2.5m Isaac Newton Telescope (only part of the CCD #4 is shown) at the Roque de los Muchachos Observatory. The following color code was used: $H\alpha$ (red), $H\beta$ (green), B (blue) (credit of the image by Ángel R. López-Sánchez, Australian Astronomical Observatory). The field-of-view of the image is $\sim 11' \times 11'$. The position of the slit used to obtain the nebular ISIS@WHT spectroscopy is shown. The PA was 320° . Slit width is not at scale.

and the red ones from $\lambda\lambda 5498$ to 9199 \AA . The seeing during the observations was $\sim 2.0''$. The exposure times were $4 \times 1200 \text{ s}$ in the blue, $3 \times 1200 \text{ s}$ in the red ($\lambda_c = 6147 \text{ \AA}$) and $1 \times 1200 \text{ s}$ in the far red ($\lambda_c = 8148 \text{ \AA}$) observations.

The spectra were wavelength calibrated with a CuNe+CuAr lamp. The correction for atmospheric extinction was performed using the average curve for continuous atmospheric extinction at Roque de los Muchachos Observatory. The absolute flux calibration was achieved by observations of the standard star BD+45 4655. We used the IRAF⁴ TWODSPEC reduction package to perform bias correction, flat-fielding, cosmic-ray rejection, wavelength and flux calibration. We checked the relative flux calibration between the bluest and reddest wavelengths by calibrating the spectrophotometric standard by itself, finding a relative flux calibration uncertainty better than $\sim 5 \%$. Fig. 2 shows an illustrative example of the quality of our nebular spectroscopic observations, where the main nebular lines used in this study are indicated. The sky emission could not be removed because the nebular emission was present along the whole slit.

⁴ IRAF is distributed by National Optical Astronomical Observatory which is operated by Association of Universities for Research in Astronomy Inc., under cooperative agreement with NSF

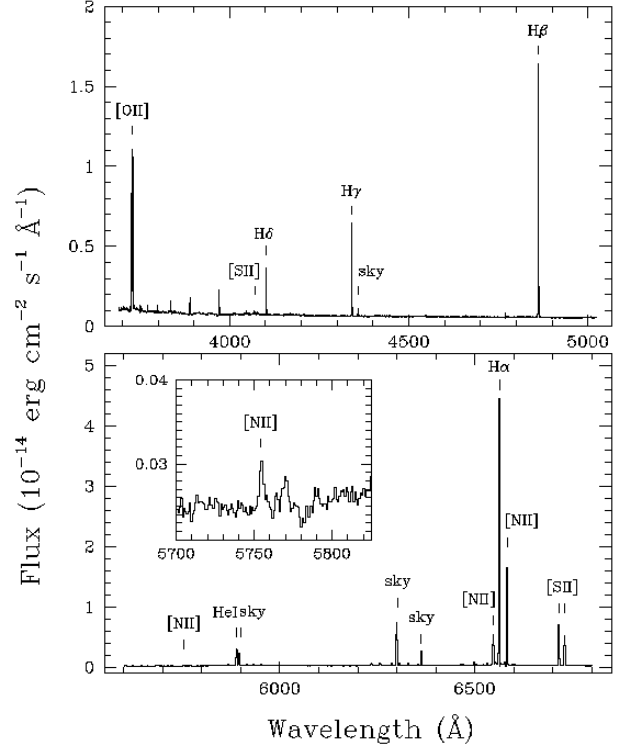


Fig. 2. Sections of the ISIS-WHT optical spectrum of the cocoon nebula (aperture #2) with some lines of interest labelled. The inset shows a zoom of the zone around $[N \text{ II}] 5755 \text{ \AA}$. The mercury Hg I 4358 \AA line and other night-sky features are also indicated. Sky emission could not be removed from the spectrum (see text).

2.2. Stellar spectroscopy

The spectroscopic observations⁵ of BD+46 3474 were carried out with the FIES (Telting et al., 2014) cross-dispersed, high-resolution echelle spectrograph attached to the 2.56m NOT telescope at El Roque de los Muchachos observatory on 2012 September 10. The low-resolution mode ($R = 25000$, $\delta\lambda = 0.03 \text{ \AA/pix}$) was selected, and the entire spectral range $3700\text{--}7100 \text{ \AA}$ was covered without gaps in a single fixed setting. We took one single spectrum with an exposure time of 1200 s . The signal-to-noise ratio achieved was above 250.

The spectrum was reduced with the FIEStool⁶ software in advanced mode. The FIEStool pipeline provided a wavelength calibrated, blaze-corrected, order-merged spectrum of high quality. This spectrum was then normalized with our own developed IDL routines. A selected range of the spectrum of BD+46 3474, where the main diagnostic lines used for the stellar parameter and abundance determination are indicated, is presented in Fig 3.

3. Empirical analysis of the nebular spectra

3.1. Aperture selection and line flux measurements

We obtained 1D spectra of zones of the nebula at different distances from the central star by dividing the long-slit used for the ISIS@WHT nebular observations in 8 apertures within the limits

⁵ The FIES spectrum of BD+46 3474 was obtained during one of the observing nights of the *IACOB spectroscopic database of Northern Galactic OB stars* program (Simón-Díaz et al., 2011a).

⁶ <http://www.not.iac.es/instruments/fies/fiestool/FIEStool.html>

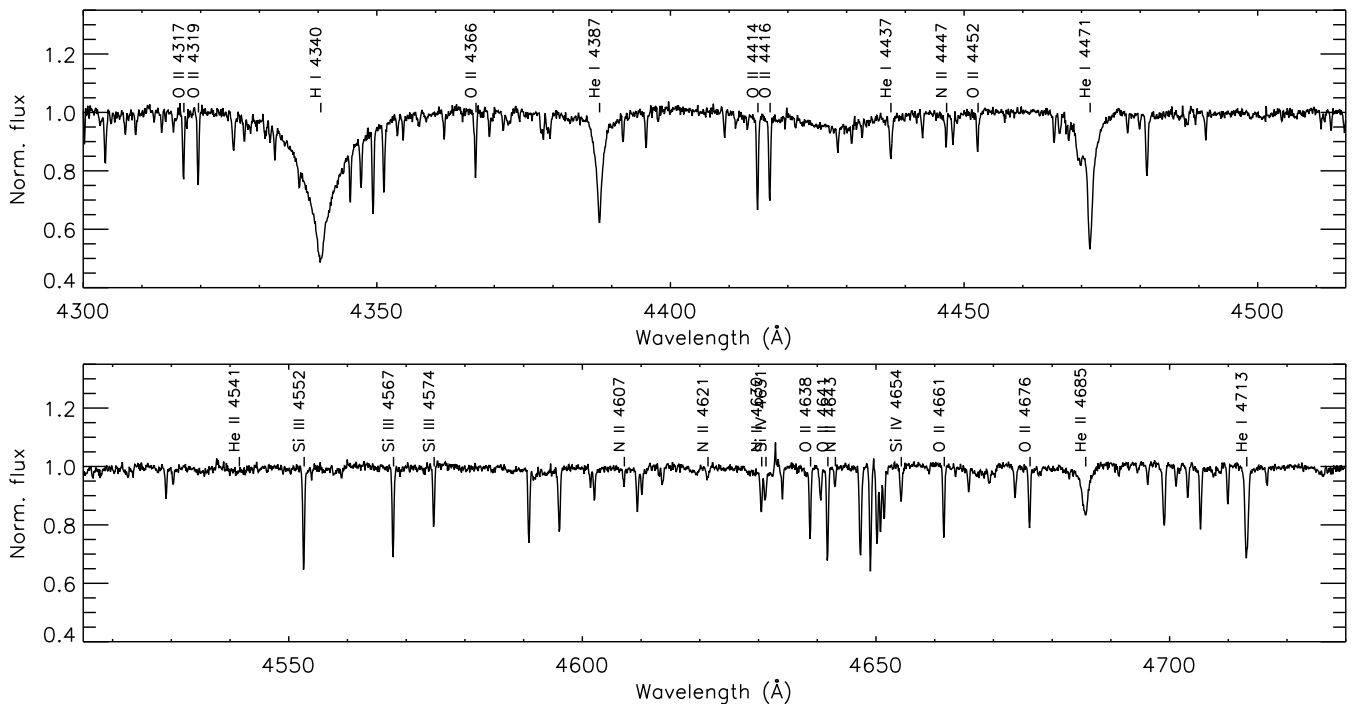


Fig. 3. Spectrum of BD+46 3474 in the region between 4300 and 4730 Å. In contrast to the broad hydrogen Balmer and He I lines (H_γ and He I $\lambda\lambda$ 4387, 4471 and 4713 in the plotted spectral window), metal lines appear very narrow due to the low $v \sin i$ of the star. Only the Si III-IV, O II and N II lines present in the plotted region and used for the spectroscopic abundance analysis are indicated in the figure (see text and Table 4).

of the nebula. Additionally we extracted a spectrum containing all the apertures to compare with the results obtained from the individual ones.

The size of the apertures, except the integrated one, was $22''$. First aperture was centered $62.8''$ away BD+46 3474 in order to avoid strong dust scattered stellar continuum. A star about $78.3''$ away BD+46 3474 was also avoided. The positions of the apertures are summarized in Table 1.

The extraction of 1D spectra from each aperture was done using the IRAF task *apall*. The same zone and spatial coverage was considered in the blue and red spectroscopic ranges.

We detected H I and He I optical recombination lines, along with collisionally excited lines (CELs) of several low ionized ions, such as [O II], [N II], [S II] and [S III]. Line fluxes were measured using the SPLIT routine of the IRAF package by integrating all the flux included in the line profile between two given limits and over a local continuum estimated by eye.

Each emission line in the spectra was normalized to a particular H I recombination line present in each wavelength interval: $H\beta$ for the blue range, $H\alpha$ for the red spectra, and P11 for the far-red spectra, respectively.

The reddening coefficient, $c(H\beta)$ was obtained by fitting the observed $H\delta/H\beta$ and $H\gamma/H\beta$ line intensity ratios –the three lines lie in the same spectral range– to the theoretical ones computed by Storey & Hummer (1995) for $T_e = 6500$ K and $n_e = 100$ cm $^{-3}$.

Finally, to produce a final homogeneous set of line intensity ratios, the red spectra were re-scaled to $H\beta$ applying the extinction correction and assuming the theoretical $H\alpha/H\beta$ and P11/ $H\beta$ ratios: $I(H\alpha)/I(H\beta) = 2.97$ and $I(P11)/I(H\beta) = 0.014$ obtained assuming $T_e = 6500$ K and $n_e = 100$ cm $^{-3}$.

3.2. Uncertainties

Several sources of uncertainties must be taken into account to obtain the errors associated with the line intensity ratios. We estimated that the uncertainty in the line intensity measurement due to the signal-to-noise of the spectra and the placement of the local continuum is typically $\sim 2\%$ for $F(\lambda)/F(H\beta) \geq 0.5$, $\sim 5\%$ for $0.1 \leq F(\lambda)/F(H\beta) \leq 0.5$, $\sim 10\%$ for $0.05 \leq F(\lambda)/F(H\beta) \leq 0.1$, $\sim 20\%$ for $0.01 \leq F(\lambda)/F(H\beta) \leq 0.05$, $\sim 30\%$ for $0.005 \leq F(\lambda)/F(H\beta) \leq 0.01$, and $\sim 40\%$ for $0.001 \leq F(\lambda)/F(H\beta) \leq 0.005$. We did not consider those lines which are weaker than $0.001 \times F(H\beta)$. Note that uncertainties indicated in Table 1 only refer to this type of errors.

By comparing the resulting flux-calibrated spectra of our standard star with the corresponding tabulated flux, we could estimate that line ratio uncertainties associated to the flux calibration is $\sim 3\%$ when the wavelengths are separated by 500–1500 Å and $\sim 5\%$ if they are separated by more than that. For the cases where the corresponding lines are separated by less than 500 Å, the uncertainty in the line ratio due to uncertainties in the flux calibration is negligible.

The uncertainty associated to extinction correction was computed by error propagation. Again, the contribution of this uncertainty to the total error is negligible when line ratios of close-by lines are considered (e.g. [S II] $\lambda 6716$ /[S II] $\lambda 6730$). The final errors in the line intensity ratios used to derive the physical properties of the nebula were computed by adding quadratically these three sources of uncertainty.

3.3. Physical conditions

Electron temperature (T_e), and density (n_e) of the ionized gas were derived from classical CEL ratios, using PyNEB, a python based code (Luridiana et al., 2012) and the set of atomic data

Table 1. Line fluxes⁽¹⁾ corrected from extinction ($H\beta=100$), and results from the empirical analysis⁽²⁾ form CELs of the nebular spectra extracted from the 8 apertures and the integrated one.

			Aperture								
			A1	A2	A3	A4	A5	A6	A7	A8	Integrated
Center position ⁽³⁾ (arcsec)			62.8	93.8	115.8	137.8	159.8	181.8	203.8	225.8	144.3
Angular area (arcsec ²)			22	22	22	22	22	22	22	22	176
λ (Å)	Ion	Mult.	$I(\lambda)/I(H\beta)$								
3726.03	[O II]	1F	74±6	72±2	73±3	80±2	94±5	93±7	107±5	129±18	80±4
3728.82	[O II]	1F	103±7	102±3	102±3	112±3	130±7	129±9	149±6	172±22	111±5
4068.60	[S II]	1F	2.5±0.5	2.6±0.3	2.8±0.5	3.1±0.4	3.2±0.3	2.8±0.6	6±1	–	2.8±0.4
4076.35	[S II]	1F	1.4±0.4	1.6±0.2	1.7±0.2	1.9±0.3	3.9±0.7	4±1	6±2	–	2.3±0.3
4101.74	H I	H δ	25±1	25.3±0.7	25.8±0.7	25.6±0.7	26±2	27±2	26±2	24±5	26±1
4340.47	H I	H γ	47±2	46±1	46±1	46±1	46±2	46±2	46±2	47±7	46±1
4861.33	H I	H β	100±2	100±2	100±2	100±2	100±2	100±2	100±2	100±2	100±2
5754.64	[N II]	3F	0.51±0.07	0.53±0.05	0.62±0.08	0.6±0.1	–	–	–	–	0.5±0.1
5875.64	He I	11	2.1±0.2	–	–	–	–	–	–	–	1.0±0.2
6548.03	[N II]	1F	36±2	35±1	38±1	37±1	39±3	41±2	39±1	42±4	37±2
6562.82	H I	H α	297±18	297±8	297±8	297±8	297±20	297±15	297±6	297±23	297±15
6583.41	[N II]	1F	111±7	108±3	109±3	113±3	115±8	122±6	124±3	121±9	111±6
6678.15	He I	46	0.44±0.06	–	–	–	–	–	–	–	–
6716.47	[S II]	2F	41±3	45±1	51±2	59±2	61±4	67±4	72±2	71±6	51±3
6730.85	[S II]	2F	30±2	33.2±0.9	38±1	43±1	44±3	49±3	52±1	50±4	37±2
8862.79	H I	P11	1.4±0.2	1.4±0.1	1.4±0.1	1.4±0.2	1.4±0.5	1.4±0.4	1.4±0.3	1.4:	1.4±0.2
9014.91	H I	P10	1.1±0.3	1.2±0.1	1.2±0.1	1.1±0.2	1.0:	0.6:	0.4:	–	1.1±0.3
9068.90	[S III]	1F	6±1	6.5±0.4	4.5±0.3	3.5±0.3	2.9±0.8	2.5±0.8	1.9±0.6	1.7:	4.4±0.6
	$c(H\beta)$		1.07±0.10	0.79±0.02	0.89±0.04	0.61±0.02	0.90±0.08	0.95±0.11	1.12±0.04	1.65±0.21	0.88±0.06
	$F(H\beta)$ ⁽⁴⁾		2.39±0.05	2.72±0.05	2.49±0.05	2.07±0.04	0.78±0.02	0.74±0.02	0.40±0.01	0.26±0.01	11.8±0.2
	n_e ([O II])		63 ⁺⁵⁹ ₋₆₃	50±28	56±35	53±25	59 ⁺¹⁰⁶ ₋₅₉	58 ⁺⁷⁶ ₋₅₈	41±29	28 ⁺¹¹⁰ ₋₂₈	60±43
	n_e ([S II])		48 ⁺⁸⁰ ₋₄₈	50±30	50±34	50±31	61±56	63 ⁺⁸⁹ ₋₆₃	63±46	90 ⁺¹⁴⁹ ₋₉₀	46 ⁺⁶⁰ ₋₄₆
	T_e ([N II])		6850±280	7020±210	7220±280	7230±420	–	–	–	–	6900±490
	T_e ([S II])		8190±810	8030±430	7700±520	7650±390	9360±820	8800±1000	12000±2500	–	8410±580
	O ⁺ /H ⁺		8.63±0.06	8.55±0.05	8.48±0.06	8.52±0.10	–	–	–	–	8.64±0.13
	N ⁺ /H ⁺		7.87±0.07	7.82±0.04	7.79±0.05	7.79±0.07	–	–	–	–	7.86±0.10
	S ⁺ /H ⁺		6.69±0.07	6.69±0.04	6.71±0.05	6.76±0.07	–	–	–	–	6.77±0.10
	S ²⁺ /H ⁺		6.30±0.12	6.17±0.07	6.10±0.08	5.99±0.11	–	–	–	–	6.15±0.15
	O/H		8.63±0.06	8.55±0.05	8.48±0.06	8.52±0.10	–	–	–	–	8.64±0.13
	N/H		7.87±0.07	7.82±0.04	7.79±0.05	7.79±0.07	–	–	–	–	7.86±0.10
	S/H		6.84±0.06	6.81±0.04	6.80±0.04	6.83±0.06	–	–	–	–	6.86±0.08

⁽¹⁾ The errors in the line fluxes only refer to uncertainties in the line measurements (see text).
⁽²⁾ n_e in cm⁻³; T_e in K; abundances in $\log(X^+/H^+)+12$.
⁽³⁾ With respect to BD+46 3474.
⁽⁴⁾ $F(H\beta)$ in $\times 10^{-14}$ erg cm² s⁻¹ and uncorrected for reddening.

shown in Table 1. We computed n_e from the [S II] $\lambda 6717/\lambda 6731$ and [O II] $\lambda 3729/\lambda 3726$ line ratios and T_e from the nebular to auroral [N II] $\lambda \lambda(6548+84)/\lambda 5754$ line ratio and from [S II] $\lambda \lambda(6717+31)/\lambda \lambda(4068+76)$.

The methodology used for the determination of the physical conditions was as follows: we assumed a representative initial value of T_e of 10000 K and compute the electron densities. Then, the value of n_e was used to compute T_e ([N II]) and/or T_e ([S II]) from the observed line ratios; for the four innermost apertures, we only assume T_e ([N II]) as valid (see below). We iterated until convergence to obtain the final values of n_e and T_e . Uncertainties were computed by error propagation. The final n_e ([O II]), n_e ([S II]), T_e ([N II]) and T_e ([S II]) estimations, along with their uncertainties are indicated in Table 1. We do not rely on the determination of T_e ([S II]) for apertures 5–7, since it is much higher than those obtained in the other apertures, giving unreasonable low values for the chemical abundances of O, N and S when used.

In general, densities derived from the [O II] line ratio are very consistent with those derived from [S II] lines for all the apertures, and additionally, they are also homogeneous for all the apertures. On the other hand, T_e 's derived from [N II] and [S II] line ratios present non negligible differences for a given aperture, especially in the inner aperture and in the total extraction. Given

Table 2. Atomic data considered in the nebular abundance analysis.

Ion	Trans. Probabilities	CELs
		Coll. strengths
N ⁺	Galavis et al. (1997)	Tayal (2011)
O ⁺	Zeippen (1982)	Pradhan et al. (2006)
S ⁺	Podobedova et al. (2009)	Ramsbottom et al. (1996)
S ²⁺	Podobedova et al. (2009)	Galavis et al. (1995)

the high dependence of the value of T_e ([S II]) with the set of collisional strengths adopted and that S⁺ zone do not strictly match with N⁺ zone (S⁺ is in the outer zones of the nebula, whereas N⁺ is probably more evenly distributed along the nebula), we decided to adopt only T_e ([N II]) as representative of the whole nebula.

3.4. Chemical abundances

We have detected only two He I lines in the innermost aperture. As hydrogen lines on this aperture could be affected by fluorescence effects (see below), we decided not computing the He⁺

abundance that should be, in any case, a very low limit of the total He abundance due to the low ionization degree of the nebula.

Ionic abundances of N^+ , O^+ , S^+ , and S^{2+} were derived from CELs, using PYNEB. We assumed a one zone scheme, in which we adopted $T_e([N II])$ to compute N^+ , O^+ , S^+ and S^{2+} abundances. We assumed the average of $n_e([S II])$ and $n_e([O II])$ as representative for each aperture. Due to the low T_{eff} of the ionizing star, we have not detected CELs of high ionization species, such as O^{2+} , Ar^{2+} or Ne^{2+} . For the same reason, $O II$ ORLs have not been detected in our spectrum. Additionally, neither the $O I$ ORLs in the 7771-7775 Å range were detected in our spectrum because they are intrinsically faint and lie in a zone with strong sky emission; therefore, we could not compute the abundance discrepancies for O^+ nor for O^{++} in this nebula (see Sect. 1).

We then derived total abundances of O, N and S for each aperture without using ionization correction factors (ICFs). We have to remark the importance of this because one of the main uncertainty sources in total abundances determinations in H II regions come from the necessity of using ICFs (see more details in Sect. 5). The ionic abundances of O^+ , N^+ , S^+ , S^{2+} , along with the total abundances of O, N and S are shown in Table 1.

From Table 1 it can be seen that both physical conditions and total chemical abundances obtained from the innermost aperture, as well as from the integrated one are somewhat different than those obtained from apertures 2, 3 and 4, which are remarkably consistent one with each other. In principle one should not expect a variation in the total abundance obtained for a given element, especially if they were derived directly from ionic abundances, without using any ICF. Ferland (1999) and Luridiana et al. (2009) described the importance of fluorescent excitation of Balmer lines due to continuum pumping in the hydrogen Lyman transitions by non-ionizing stellar continua. In particular, Luridiana et al. (2009) performed a detailed description of this effect and its behaviour with the spectral type, luminosity class, and the distance to the star for environments where Lyman transitions are optically thick. In our case, this effect can be particularly important in aperture 1, which is the closest to the star. This effect depends on several parameters and it can only be addressed with a detailed photoionization model with an appropriate high resolution sampling of the non-ionizing spectrum of the stellar source (Luridiana et al., 2009). From a qualitative approach, differential fluorescent excitation of H I lines can affect mainly the determination of the extinction coefficient, $c(H\beta)$, which can be overestimated in the apertures closest to the ionizing star (Simón-Díaz et al., 2011b, reported this effect in the inner apertures of a longslit study of M 43); the overall effect would be i) an overestimation of the line fluxes bluer to $H\beta$ in the blue range, ii) an underestimation of line fluxes in the far-red range, and iii) an overestimation/underestimation of fluxes for lines bluer/redder to $H\alpha$, respectively, in the red range. This effect would only affect substantially O^+/H^+ abundances because $[O II]$ line fluxes would be overestimated. The effect in N^+ would be very small, given the proximity of these lines to $H\alpha$. Sulphur ionic abundances are affected by ionization structure effects and can not be discussed on these terms. On the other hand, the effect in the determination of n_e would be negligible because, both $n_e([O II])$ and $n_e([S II])$ are computed from line ratios belonging to the same range and very close in wavelength; finally, a small effect would emerge in the determination of $T_e([N II])$, mainly due to the difference in wavelength between auroral and nebular $[N II]$ lines. Taking into account all these possible effects, hereinafter we will not consider aperture 1 computations given the remarkable differences with apertures 2, 3 and 4, and we will

consider the weighted average of these three apertures as representative of the whole nebula.

In last column of Table 1, for comparative purposes, we also present the results for the integrated spectra. The results obtained for the integrated spectra are very similar to those obtained in aperture 1. This is probably due to the effect of apertures 5 to 8 in the collapsed spectrum; these four apertures show higher values of $c(H\beta)$ than apertures 2 to 4, hence, mimicking the effect observed in aperture 1.

4. Quantitative spectroscopic analysis of BD+46 3474

We followed a similar strategy as described in Simón-Díaz (2010) to perform a detailed, self-consistent spectroscopic abundance analysis of BD+463474 by means of the modern stellar atmosphere code FASTWIND (Santolaya-Rey et al., 1997; Puls et al., 2005). In brief, the stellar parameters were derived by comparing the observed H Balmer line profiles and the ratio of Si III-IV line equivalent widths (EWs) with the output from a grid of FASTWIND models. Then, the same grid of models was used to derive the stellar abundances by means of the curve-of-growth method.

The projected rotational velocity ($v \sin i$) of the star was derived by means of the *iacob*-broad procedure implemented in IDL (see notes about its performance in Simón-Díaz & Herrero, 2014) and the measurement of the equivalent width of the metal lines of interest was performed as described in Simón-Díaz (2010). While Simón-Díaz (2010) concentrated in the oxygen and silicon abundance determination, in the present study we were able to also extend the abundance analysis to nitrogen, taking advantage of the implementation of a new nitrogen model atom into the FASTWIND code (Rivero González et al., 2011, 2012).

In a first step we used the $H\gamma$ line, along with the ratio $EW(Si IV \lambda 4116)/EW(Si III \lambda 4552)$ to constrain the effective temperature and gravity, obtaining 30100 ± 500 , 30500 ± 500 , and 30800 ± 700 K for $\log g = 4.1$, 4.2, and 4.3 dex, respectively (with $\log g = 4.2$ dex providing the best *by-eye* fit to $H\gamma$). An independent determination of these two parameters, together with the helium abundance (Y_{He}), the microturbulence (ζ_t), and the wind-strength Q-parameter ($\dot{M} (R v_\infty)^{-3/2}$, Puls et al. 1996) was obtained by performing a HHe spectroscopic analysis using the *iacob*-gbat package (Simón-Díaz et al., 2011a). In this case we used the full set of H and He I-II lines available in the FIES spectrum, obtaining a perfect agreement with the results from the HSi analysis ($T_{\text{eff}} = 30100 \pm 1000$ K and $\log g = 4.2 \pm 0.1$ dex), plus $Y_{\text{He}} = 0.11 \pm 0.02$, $\zeta_t < 5$ km s $^{-1}$, and $\log Q < -13.5$.

The final set of stellar parameters derived spectroscopically (along with the corresponding uncertainties) is summarized in Table 3. For completeness, we also include in Table 3 the derived Si, O and N abundances (see below) as well as other stellar parameters of interest for further studies of the Cocoon nebula and its ionizing source such as the radius, luminosity and spectroscopic mass (see notes about how these parameters were derived in Appendix A). The spectroscopic parameters were then fixed for the subsequent Si, O and N abundance analysis. We present in Table 4 the considered set of Si III-IV, O II, and N II-III diagnostic lines, along with the measured equivalent widths and corresponding line-by-line abundances⁷ (plus the associated uncertainties). The same information is represented graphically in Figure 4.

⁷ $\epsilon_X = \log(X/H) + 12$

Table 3. First and second columns: Spectroscopic parameters and abundances of Si, O, and N derived through the FASTWIND analysis of the optical spectrum of BD +463474. Third and fourth columns: Some photometric quantities used to compute the physical parameters of the star are also presented for completeness.

T_{eff} (K)	30500 ± 1000	V	9.74
$\log g$ (dex)	4.2 ± 0.1	(B-V)	0.78
Y(He)	0.11 ± 0.02	(B-V) ₀	-0.27
$\log Q$	< -13.5	E(B-V)	1.05
ζ_t (km s ⁻¹)	< 5	A_V	3.25
$v \sin i$ (km s ⁻¹)	< 15	M_V	-3.0 ⁽¹⁾
$\log(\text{Si}/\text{H})+12$	7.51 ± 0.05	R (R _⊙)	5.2 ± 0.2 ⁽¹⁾
$\log(\text{O}/\text{H})+12$	8.73 ± 0.08	$\log L/L_{\odot}$	4.29 ± 0.03 ⁽¹⁾
$\log(\text{N}/\text{H})+12$	7.86 ± 0.05	M_{sp} (M _⊙)	15 ± 2 ⁽¹⁾

⁽¹⁾ Corresponding to a distance of 800 pc (see notes in Appendix A).

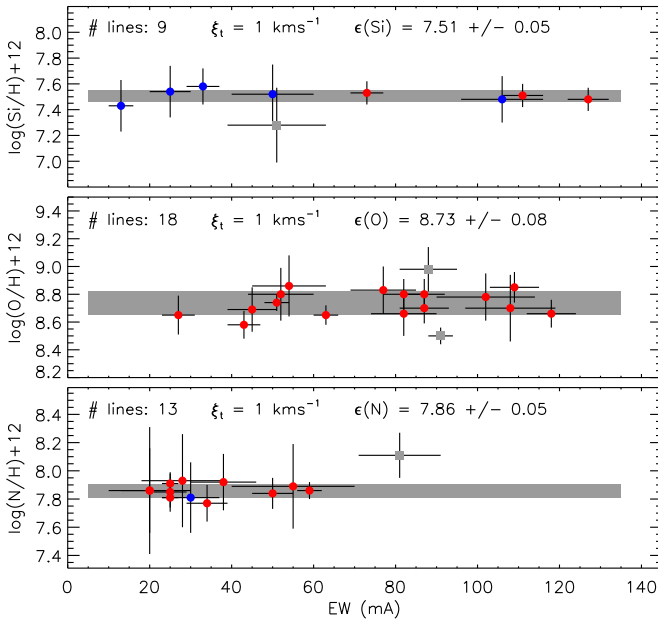


Fig. 4. Final $\log(X/H)$ vs. EW diagrams for Si, O, and N, resulting from the abundance analysis of BD +46 4374. The microturbulence providing a minimum dispersion of line-by-line abundances is indicated at the top of each panel along with the associated mean and abundance dispersion. Red and blue dots indicate lines from different ions (red dots: Si III, O II and N II; blue dots: Si IV and N III); grey dots correspond to those lines excluded from the analysis (see also Sect. 4 and Table 4). The grey horizontal band correspond to the adopted value and its uncertainty.

In the three cases, a very low value of microturbulence ($\zeta_t = 1 \pm 1$ km s⁻¹) is required to obtain a zero slope in the ϵ_X – EW diagrams. We have marked in bold, and as grey squares in Figure 4, those lines whose abundances deviates more than 2σ from the resulting distribution of abundances. These lines were excluded from the final computation of mean abundances – ϵ_X – and standard deviations – $\Delta\epsilon_X(\sigma)$ –. We also indicate in Table 4 the uncertainty associated with a change of ± 1 km s⁻¹ in microturbulence – $\Delta\epsilon_X(\zeta_t)$ – and, for the case of oxygen, the effect of modifying T_{eff} and $\log g$ in ± 1000 K and 0.1 dex, respectively – $\Delta\epsilon_X(\text{SP})$ –.

Table 4. Results from the abundance analysis of BD +463474 (B0.5 V). Values in bold indicate lines whose abundances deviates more than 2σ from the resulting distribution of abundances.

BD +463474	$T_{\text{eff}} = 30500$ K, $\log g = 4.2$ dex			$\zeta_t(\text{Si})=1$
Line	EW (mÅ)	ΔEW (mÅ)	ϵ_{Si} (dex)	$\Delta\epsilon_{\text{Si}}$ (dex)
Si III $\lambda 4552$	127	5	7.48	0.09
Si III $\lambda 4567$	111	5	7.51	0.09
Si III $\lambda 4574$	73	4	7.53	0.09
Si IV $\lambda 4116$	106	10	7.48	0.18
Si IV $\lambda 4212$	33	4	7.58	0.14
Si IV $\lambda 4631$	50	10	7.52	0.23
Si IV $\lambda 4654$	51	12	7.28	0.29
Si IV $\lambda 6667$	13	3	7.43	0.20
Si IV $\lambda 6701$	25	5	7.54	0.20

$$\Delta\zeta_t(\text{Si}) = 1 \Rightarrow \begin{matrix} \epsilon_{\text{Si}} = \mathbf{7.51} \\ \Delta\epsilon_{\text{Si}}(\sigma) = 0.05 \\ \Delta\epsilon_{\text{Si}}(\zeta_t) = 0.06 \end{matrix}$$

BD +463474	$T_{\text{eff}} = 30500$ K, $\log g = 4.2$ dex			$\zeta_t(\text{O})=1$
Line	EW (mÅ)	ΔEW (mÅ)	ϵ_{O} (dex)	$\Delta\epsilon_{\text{O}}$ (dex)
O II $\lambda 3945$	54	9	8.86	0.22
O II $\lambda 3954$	77	8	8.83	0.17
O II $\lambda 4317$	102	12	8.78	0.17
O II $\lambda 4319$	87	6	8.70	0.11
O II $\lambda 4366$	82	8	8.66	0.16
O II $\lambda 4414$	118	6	8.66	0.10
O II $\lambda 4416$	109	6	8.85	0.11
O II $\lambda 4452$	52	8	8.80	0.19
O II $\lambda 4638$	88	7	8.98	0.16
O II $\lambda 4641$	91	3	8.50	0.06
O II $\lambda 4661$	87	5	8.80	0.11
O II $\lambda 4676$	82	5	8.80	0.11
O II $\lambda 6721$	51	3	8.74	0.06
O II $\lambda 4076$	108	11	8.70	0.24
O II $\lambda 4891$	27	4	8.65	0.14
O II $\lambda 4906$	45	6	8.69	0.16
O II $\lambda 4941$	43	4	8.58	0.10
O II $\lambda 4943$	63	3	8.65	0.07

$$\begin{matrix} \Delta\zeta_t(\text{O}) = 1 \\ \Delta T_{\text{eff}} = 1000, \Delta \log g = 0.1 \end{matrix} \Rightarrow \begin{matrix} \epsilon_{\text{O}} = \mathbf{8.73} \\ \Delta\epsilon_{\text{O}}(\sigma) = 0.08 \\ \Delta\epsilon_{\text{O}}(\zeta_t) = 0.03 \\ \Delta\epsilon_{\text{O}}(\text{SP}) = 0.08 \end{matrix}$$

BD +463474	$T_{\text{eff}} = 30500$ K, $\log g = 4.2$ dex			$\zeta_t(\text{N})=1$
Line	EW (mÅ)	ΔEW (mÅ)	ϵ_{N} (dex)	$\Delta\epsilon_{\text{N}}$ (dex)
N II $\lambda 3995$	81	10	8.11	0.16
N II $\lambda 4607$	20	10	7.86	0.45
N II $\lambda 4621$	20	7	7.86	0.30
N II $\lambda 4630$	55	15	7.89	0.30
N II $\lambda 4643$	25	2	7.81	0.07
N II $\lambda 4447$	38	8	7.92	0.20
N II $\lambda 5045$	28	10	7.93	0.33
N II $\lambda 5666$	34	5	7.77	0.13
N II $\lambda 5676$	25	2	7.91	0.07
N II $\lambda 5679$	59	3	7.86	0.06
N II $\lambda 5007$	25	4	7.85	0.14
N II $\lambda 5005$	50	5	7.84	0.11
N II $\lambda 4634$	30	7	7.81	0.25

$$\Delta\zeta_t(\text{N}) = 1 \Rightarrow \begin{matrix} \epsilon_{\text{N}} = \mathbf{7.86} \\ \Delta\epsilon_{\text{N}}(\sigma) = 0.05 \\ \Delta\epsilon_{\text{N}}(\zeta_t) = 0.02 \end{matrix}$$

5. Discussion

5.1. Nebular and stellar abundances: Cocoon vs. Orion and M43

The study of interstellar absorption lines of the cold gas by Sofia & Meyer (2001) demonstrated that the local ISM out to 1.5 Kpc from the Sun is chemically homogeneous to the 10% level. A similar result has been more recently obtained by Nieva & Przybilla (2012) from a very thoughtful abundance analysis of a sample of 29 early B-type stars located 500 pc around the Sun. Given its distance to the Sun (~ 1 Kpc), the Cocoon nebula and BD+46 3474 are expected to share the same chemical composition as the Orion nebula ($d \sim 450$ pc) and other B-type stars in the Solar vicinity. For a discussion about the comparison of chemical abundances from B-type stars in the solar

Table 5. Comparison of derived stellar and gas-phase nebular abundances obtained for the Cocoon nebula, M43 and the Orion nebula. All the CEL abundances are for $t^2 = 0$. Abundances from other B-type stars in the Solar neighborhood are also quoted for reference.

	Cocoon ^a		Orion		M43	Solar neighborhood
	Nebular (CEL)	B stars	Nebular (CEL) ^b	B stars	Nebular (CEL) ^f	B stars ^g
Si	–	7.51±0.05	–	7.51 ^c /7.50 ^d ±0.05	–	7.50±0.05
O	8.52±0.05	8.73±0.08	8.54±0.03	8.73 ^c /8.77 ^d ±0.04	8.53±0.09	8.76±0.05
N	7.81±0.03	7.86±0.05	7.73±0.09	7.82 ^d ±0.07	7.82±0.04	7.79±0.04
S	6.81±0.04	–	6.83±0.04	7.15 ^e ±0.05	6.95±0.09	–

Notes: ^(a) This work; ^(b) Reanalysis of the Orion nebula spectrum by Esteban et al. (2004) using the same atomic dataset as in this work (see Table 2); ^(c) Simón-Díaz (2010), similar analysis as in this work using FASTWIND; ^(d) Nieva & Simón-Díaz (2011), reanalysis of the spectra from Simón-Díaz (2010) using similar techniques as in Nieva & Przybilla (2012); ^(e) Daflon et al. (2009); ^(f) Reanalysis of M43 spectrum by Simón-Díaz et al. (2011b) using the same atomic dataset as in this work; ^(g) Nieva & Przybilla (2012).

neighbourhood and abundances obtained in the Sun, we refer the reader to the study of Nieva & Przybilla (2012) who made this comparison in the framework of recent observational data and Galactic chemical and kinematical evolution models.

In the first two columns of Table 5 we present a summary of the Cocoon gas-phase nebular and stellar abundances that will be considered hereafter. As discussed in Sect. 3.4, we will assume the weighted average of the gas-phase abundances for apertures 2 to 4 as representative of the nebula. For comparative purposes, we also quote:

- the N, O and S abundances resulting from a reanalysis of the Orion nebula and M43 spectra presented in Esteban et al. (2004) and Simón-Díaz et al. (2011a) using the same atomic dataset as in this paper;
- the Si, O, and N abundances derived by Simón-Díaz (2010), Nieva & Simón-Díaz (2011) for B-type stars in the Orion star forming region and by Nieva & Przybilla (2012) for B-type stars in the Solar vicinity; and
- the S abundances derived by Daflon et al. (2009) for B-type stars in the Orion star forming region.

The agreement between the Si, O and N abundances derived from the spectroscopic analysis of BD+46 3474 and the recent determinations of abundances in B-type stars in the Orion OB1 association and, more generally, the solar neighborhood is quite remarkable.

The comparison of gas-phase abundances in the Cocoon nebula and the Orion star-forming region (Orion nebula+M43) is also almost perfect when the same atomic datasets are used (see, however, the effect of assuming different available atomic data for sulphur in Sect. 5.2). Particularly, the comparison with the results obtained for M43 is of special interest, owing to no ICFs are needed for computing O, N and S abundances in M43 (see Simón-Díaz et al., 2011b). Using the same atomic dataset than in this work, the abundances of O and N are in excellent agreement between both nebulae (see Table 5). The differences between S abundances in the Cocoon nebula and in M43 cannot be attributed to atomic data, nor to the use of an ICF; however, we have used different lines for computing S^{2+}/H^+ ratio: in the Cocoon nebula we used the bright nebular lines at $\lambda\lambda 9069, 9531$ while in M43⁸ we used the faint and extremely temperature dependent auroral line at $\lambda 6312$. As we have assumed the same temperature for S^+ and S^{2+} regions ($T_e([N II])$) for the Cocoon

nebula and $T_e([O II])$ for M43), differences in the true temperature in the zones where the different ions are present may explain the observed discrepancy. This fact remarks the importance of using consistent sets of lines, physical conditions, atomic data and ICFs when comparing abundances obtained for the same element in different objects.

In the case of the Orion nebula, there is a small difference between N abundances, which may be perfectly explained due to uncertainty in the ICF(N) which has to be assumed for the case of the Orion nebula. Indeed, we only indicate in Table 5 the value provided by García-Rojas & Esteban (2007); however, Esteban et al. (2004) and Simón-Díaz & Stasińska (2011) proposed another two possible values of the total gas-phase N abundance in the Orion nebula (7.65 ± 0.09 and 7.92 ± 0.09 , respectively). The three values result from the analysis of the same spectrum but a different assumption of the ICF(N). In this context, we highlight the importance of the Cocoon nebula and M43 for the comparison of nitrogen abundances derived from the analysis of the nebular and stellar spectra (Sect. 5.2), since in these cases no ICF(N) is needed to obtain the total nebular nitrogen abundance. The results obtained for these two nebulae strongly favour the ICF(N) used by García-Rojas & Esteban (2007) for computing total N abundance in the Orion nebula.

5.2. Nebular vs. stellar abundances in the Cocoon nebula

Before starting the comparison of nebular and stellar abundances in the Cocoon nebula, we want to briefly summarize the main results of a similar study performed by Simón-Díaz & Stasińska (2011) in the Orion star forming region. They used the chemical abundance study of the Orion star forming region from B-type stars (Simón-Díaz, 2010; Nieva & Simón-Díaz, 2011) to compare the derived abundances with those obtained for non-refractory elements (C, N, O and Ne) in the most detailed study of the gas-phase chemical abundances on the Orion nebula (Esteban et al., 2004). The main conclusion of these authors is that oxygen abundance derived from CELs (corrected from depletion onto dust grains) in the Orion nebula is irreconcilable with that derived from B-type stars. On the other hand, they find that N and Ne gas phase abundances and C gas phase+dust abundances from CELs seemed to be consistent with those derived in B-type stars (see Fig. 1 of Simón-Díaz & Stasińska, 2011). In addition, these authors find that oxygen gas phase+dust abundances derived from optical recombination lines (ORLs) agree very well with oxygen abundances derived in the stars.

In the study of the Cocoon nebula presented here we concentrate on the comparison of nebular and stellar abundances

⁸ The spectra of M43 used by Simón-Díaz et al. (2011b) do not cover the near infrared zone of the spectrum where the bright nebular [SIII] lines lie.

for O, N and S. As indicated in Sects. 3.4 and 5.1, one important point of this study (compared to the case of the Orion nebula) is that the total abundances of the three investigated elements are obtained without the necessity of any ICF. Although we only have access to nebular abundances derived from CELs (no ORLs are detected), we will also include in our discussion how CEL abundances corrected from the presence of possible temperature fluctuations compare to the stellar ones. In particular, since we cannot directly compute the t^2 parameter from our observations, we will assume two cases: a canonical value of $t^2=0.035$ (which is an average value in Galactic H II regions, see García-Rojas & Esteban, 2007), and the value derived for the Orion nebula ($t^2=0.022$, Esteban et al., 2004).

A meaningful comparison of nebular and stellar abundances first requires the nebular gas-phase abundances (Tables 1 and 5) to be corrected from possible depletion onto dust grains. Several authors have estimated the oxygen depletion factor in the Orion nebula by comparing abundances of the refractory elements Mg, Si and Fe in the gas phase with those found in the atmospheres of B stars of the Orion cluster (e.g. Esteban et al., 1998; Mesa-Delgado et al., 2009a; Simón-Díaz & Stasińska, 2011); these authors found oxygen depletions between 0.08 and 0.12 dex. For a detailed discussion on the computations of such depletions, we refer the reader to Simón-Díaz & Stasińska (2011). Lacking for the whole bunch of information needed to perform a similar computation in the Cocoon nebula, we decided to adopt a canonical value of 0.10 dex as representative of the oxygen depletion in this nebula and consider an associated uncertainty of ± 0.02 dex. Nitrogen is expected not to be a major constituent of dust in H II regions (Jenkins, 2014); therefore, no correction is needed. For sulphur, the situation is more complicated; although for a long time sulphur was thought not to be depleted onto dust grains (see e.g. Sofia et al., 1994), recently, some authors (Jenkins, 2009; White & Sofia, 2011) drew attention about the risks of assume sulphur as a standard for what should be virtually zero depletion, especially for some sight lines. Unfortunately, there is a lack of quantitative studies on the sulphur depletion onto dust grains, that makes this an open question that needs to be addressed in the future by using high-quality interstellar abundance measurements. We hence assume no dust correction for sulphur, but keep in mind the abovementioned argument.

5.2.1. Oxygen

Similarly to the case of the Orion nebula, the derived gas+dust oxygen abundance resulting from CELs and a $t^2=0$ (8.62 ± 0.05) is remarkably different to the O abundance obtained from the spectroscopic analysis of the central star. If we consider as valid the assumption that temperature fluctuations are affecting the determination of ionic chemical abundances using CELs (Peimbert, 1967; Peimbert & Costero, 1969), and the canonical value of $t^2=0.035$ we would obtain that total gas+dust nebular abundance would reach $12+\log(\text{O}/\text{H})=8.86$, which is now much larger than that obtained from stars. While this result could be used as an argument against the temperature fluctuation scheme, we must remind that we considered a value of t^2 that may not be representative of the actual value in the Cocoon nebula. In particular, if the value of t^2 derived for the Orion nebula is considered (0.022), the resulting gas+dust oxygen abundance would be $12+\log(\text{O}/\text{H})=8.75$, in much better agreement with the stellar one.

5.2.2. Nitrogen

As Simón-Díaz & Stasińska (2011) argued, if the RL-CEL abundance discrepancy were caused by temperature fluctuations, as suggested by Peimbert et al. (1993), one should observe the same kind of bias in the CEL abundances of the other elements. They do not find other elements such as N, C and Ne following the same behaviour as oxygen; however, they also claim that the derived total gas-phase abundances of C, N and Ne in the Orion nebula are much less accurate. This is mainly due to the uncertainties on the adopted ICFs. In the Cocoon nebula, no ICF correction is needed to be applied to compute the total N gas-phase abundance. This is due to the low excitation of the nebula, that prevents the ionization of N^+ to N^{2+} . From the comparison of the total nebular N abundance obtained from CELs (and $t^2=0$), $12+\log(\text{N}/\text{H})=7.81 \pm 0.03$ and that obtained from the analysis of the central star, $12+\log(\text{N}/\text{H})=7.86 \pm 0.05$, we can conclude that the stellar one is slightly higher but both values are consistent within the uncertainties. In this case, the CEL+ t^2 abundances that result from assuming a $t^2=0.035$ (canonical) or 0.022 (Orion nebula) are 8.02 and 7.93, respectively⁹. The later option is also in agreement with the stellar solution.

For completeness in this section we must write a word of caution regarding the stellar nitrogen abundance. Spectroscopic analysis of early-B type main sequence stars in the last years have shown an increasing observational evidence of the existence of a non-negligible percentage of narrow lined (low $v \sin i$, but not necessarily fast rotators seen pole-on) targets among these stars showing nitrogen enhancement in their photospheres (e.g., Morel et al., 2006; Hunter et al., 2008). This result warns us about the danger of extracting any conclusion from the direct comparison of nebular and stellar abundances based in one target. We hence must consider the derived nitrogen abundance in BD+46 3474 as an upper limit to be compared with the nebular abundance, specially in view of the nitrogen abundance obtained for this star in comparison with other stars in the solar neighborhood (see Table 5).

5.2.3. Sulphur

Given the low excitation of the Cocoon nebula, that prevents the presence of ionization species of S higher than S^{2+} , we skip the uncertainty associated with the use of an ICF to compute the total nebular sulphur abundance.¹⁰ However, there are still a couple of issues that makes the comparison of nebular and stellar abundances for this element still uncertain. First, the remarkable difference in the computed abundances when assuming different atomic datasets. To illustrate this we have recomputed the Cocoon nebular sulphur abundance using the same atomic data for this element as García-Rojas & Esteban (2007)¹¹. Although it was not commented in Section 5.1, the value proposed by

⁹ Note that the correction to the abundances derived from [N II] CELs is much lower than that derived from [O II] CELs. In particular, this correction depends on the wavelength of the used lines for abundance calculations, being larger for bluer lines, such as [O II] $\lambda\lambda 3726+29$ and lower for redder lines, such as [N II] $\lambda\lambda 6548+83$.

¹⁰ Taking into account the lack of O^{2+} in the nebula, and the similarity between ionization potentials of O^+ (35.12 eV) and S^{2+} (34.83 eV), this seem to be a reasonable conclusion.

¹¹ The atomic dataset used by these authors was the following: Collision strengths by Ramsbottom et al. (1996) for S^+ and Tayal & Gupta (1999) for S^{2+} . Transition Probabilities by Keenan et al. (1993) for S^+ and Mendoza & Zeippen (1982) and Kaufman & Sugar (1986) for S^{2+}

these authors for the sulphur abundance in the Orion nebula was 7.04 ± 0.04 , a factor 1.6 larger than the abundance indicated in Table 5. In the case of the Cocoon nebula, the abundance is modified from 6.81 to 6.90 (i.e. 20% difference). Second, as discussed above, there are doubts about the depletion of sulphur on dust (Jenkins, 2009) and some amount of it may be in the form of dust grains. In addition, we still do not have implemented and tested a sulphur model atom to be used with FASTWIND and could not derive the S abundance associated with BD+46 3474; however, given the good match between the Si, O and N abundances in BD+46 3474 and other stars B-type in the Orion star forming region (Sect. 5.1) we consider as a still valid exercise the comparison of our nebular sulphur abundance with those obtained by Daflon et al. (2009)¹².

From the comparison of the sulphur abundances presented in Table 5 we can conclude that there is a clear discrepancy (by more than 0.3 dex) between the nebular CEL ($t^2=0$) and stellar abundances. If we consider the presence of temperature fluctuations, and assume the canonical value for Galactic H II regions and that of the Orion nebula, we would overcome a large part of the discrepancy, reaching to values of $12+\log(\text{S}/\text{H})=7.07$ and 6.96 , respectively (to be compared with 7.15 ± 0.05). While these values are in much better agreement with the stellar abundance, the $t^2=0.022$ solution (the one for which we find better agreement in the case of O and N) is still far away from the value resulting from the analysis of the stellar spectra.

Interestingly, a perfect agreement between nebular and stellar sulphur abundances would be obtained if the atomic dataset considered by García-Rojas & Esteban (2007) is assumed and combined with a $t^2=0.035$. However, while still a valid option, this possibility is highly speculative and far from being considered as a valid scientific argument supporting any conclusion.

5.2.4. Final remarks

In Fig. 5 we illustrate all the discussion above showing the comparison between the abundances of O, N and S in the Cocoon nebula obtained using CELs and $t^2 = 0$ (blue boxes), CELs and $t^2 = 0.022$ (the Orion nebula value, red boxes) and CELs and $t^2 = 0.035$ (canonical t^2 value for Galactic H II regions, magenta) with the abundances in the central star BD+46 3474 (green boxes). For comparison we also represent the values for CELs and $t^2 = 0$ and $t^2 = 0.022$ as well as oxygen ORLs values (cyan box) for the Orion nebula. The height of the boxes represents the adopted uncertainties. All these numbers are summarized in Table 6. As a general result, for O and N, it is clear that abundances considering small temperature fluctuations ($t^2 = 0.022$, similar to what found in the Orion nebula) agree much better with what obtained from stars than those considering pure CELs with $t^2 = 0$. On the other hand, typical values of $t^2 = 0.035$ found in Galactic H II regions seem to overestimate nebular O and N abundance. As representative of the ICF problem, in Fig. 5 we show two values of the Orion N abundance, assuming the ICF by García-Rojas & Esteban (2007) (left) and Simón-Díaz & Stasińska (2011) (right); it is evident that by using different ICFs one can reach radically different conclusions.

In the case of sulphur, the situation is puzzling. Although some increase of the S abundance owing to depletion onto dust

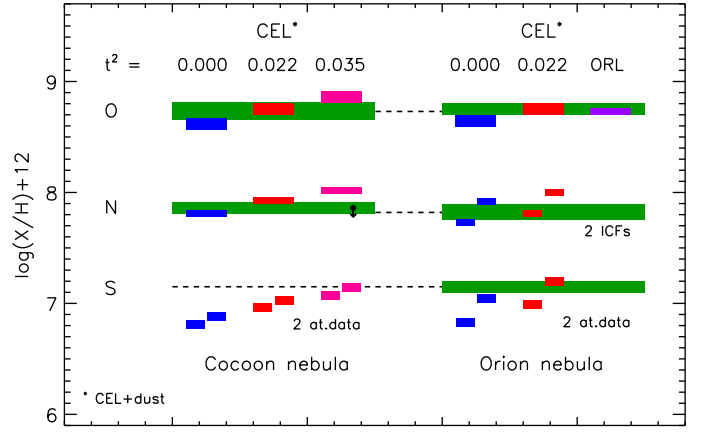


Fig. 5. Comparison of O, N, and S abundances obtained from B-type stars (green) and nebular (gas+dust) abundances derived from CEL and different values of t^2 (blue, red, and magenta). Violet box indicates O abundance obtained from ORLs in the Orion nebula by Esteban et al. (2004). The height of the boxes represents the uncertainties. Left and right columns corresponds to the Cocoon nebula and the Orion nebula, respectively. For sulphur, the resulting abundances using two different atomic dataset are indicated; for nitrogen in the Orion nebula, the abundances computed by assuming two different ICFs are shown. See text for more details.

can not be ruled out, it seems that the results for CELs and $t^2 = 0$ are far from stellar abundances. Additionally, the abundances are highly dependent on the selected atomic dataset (especially for the Orion nebula where S^{2+} is dominant). We have computed sulphur nebular abundances using atomic data from Table 2 (left) and atomic data used in García-Rojas & Esteban (2007). In general, by using the atomic dataset of Table 2, sulphur nebular abundances are going to be far from the stellar results assuming $t^2 = 0.022$ in both, the Cocoon and the Orion nebula, but can be in agreement assuming $t^2 = 0.035$, which has been considered too high from the analysis of O and N data. On the other hand, assuming the atomic dataset of García-Rojas & Esteban (2007) the situation changes and then one can reconcile sulphur nebular and stellar abundances by assuming $t^2 = 0.022$. Of course, this result do not necessarily favours one given dataset, but warns about the influence of atomic data in our results (see Luridiana et al., 2011; Luridiana & García-Rojas, 2012, for a critical review on the use of nebular atomic data).

All the results above do not necessary imply the existence of such temperature fluctuations, whatever the physical origin of such fluctuations, but they warn us about the use of pure CELs as a proxy for computing chemical abundances in photoionized regions. Additionally special care should be taken into account when selecting an ICF scheme and/or an atomic dataset, owing to a bad choice could reach to large uncertainties on the nebular chemical abundances and hence, to incorrect interpretations.

We have to emphasize the importance of including more elements to compare in future studies (mainly C, Ne and Ar). The main problem with these elements is that we would always need an ICF to compute the total nebular abundance from optical spectra. This problem may be circumvent using multiwavelength studies including UV and IR lines, but this is very difficult for very extended objects, such as Galactic H II regions owing to the different apertures used for UV, optical and IR spectrographs, which may introduce non-negligible ionization structure effects. A detailed set of photoionization models covering as much as

¹² A more recent paper by Irrgang et al. (2014) include three of the Orion stars analyzed in Simón-Díaz (2010) using a similar technique and atomic data as Nieva & Simón-Díaz (2011). The resulting sulphur abundances are in good agreement with the values obtained by Daflon et al. (2009).

Table 6. Summary of the abundances presented in Figure 5 .

	Cocoon				Orion			
	Nebular gas+dust (CEL)			B stars	Nebular gas+dust (CEL)		Nebular gas+dust (ORL)	B stars
	$t^2=0.00$	$t^2=0.022$	$t^2=0.035$		$t^2=0.00$	$t^2=0.022$		
O	8.62±0.05	8.75±0.05	8.86±0.05	8.73±0.08	8.64±0.03	8.75±0.03	8.73±0.03	8.75±0.05
N	7.81±0.03	7.93±0.03	8.02±0.03	7.86±0.05	7.73/7.92±0.03 ¹	7.81/8.00±0.03 ¹	–	7.82±0.07
S	6.81/6.88±0.04 ²	6.96/7.03±0.04 ²	7.07/7.14±0.04 ²	–	6.83/7.04±0.04 ²	6.99/7.20±0.04 ²	–	7.15±0.05

¹ Two ICFs used (see text).

² Two sets of atomic data used (see text).

possible the H II regions parameter space is needed to build a consistent set of ICFs, as it has been recently done for planetary nebulae by Delgado-Inglada et al. (2014).

6. Summary and conclusions

The Cocoon Nebula (IC 5146) –a roundish H II region ionized by a single B0.5 V star (BD+46 3474)– seems to be an ideal object to compare stellar and nebular chemical abundances and then check the abundance determinations methods in the field of H II regions and massive stars.

We collect a set of high quality observations comprising the optical spectrum of BD+46 3474 (the main ionizing source), along with long-slit spatially resolved nebular spectroscopy of the nebula .

In this paper we present the nebular abundance analysis of the spectra extracted from apertures located at various distances from the central star in the Cocoon nebula, as well as a quantitative spectroscopical analysis of the ionizing central star BD+46 3474.

We performed a detailed nebular empirical analysis of 8 apertures extracted from a long-slit located to the north-west of BD+46 3474. We obtained the spatial distribution of the physical conditions (temperature and density) and ionic abundances of O⁺, N⁺, S⁺ and S²⁺. Owing to the extremely low ionization degree of the Cocoon nebula, we can determine total abundances directly from observable ions, eliminating the uncertainties resulting of assuming an ICF scheme, which are especially significant for the case of N. In particular, the N abundance is in complete agreement with that determined by Simón-Díaz et al. (2011b) for M 43, a local H II region with a similar low ionization degree.

By means of a quantitative spectroscopic analysis of the optical spectrum of BD+46 3474 with the stellar atmosphere code FASTWIND we derived for this B0.5 V star T_{eff} = 30500±1000 K and log g = 4.2±0.1. and chemical abundances of Si, O and N (in 12+log(X/H)) of 7.51±0.05, 8.73±0.08 and 7.86±0.05, respectively.

From the comparison of O, N and S abundances in the nebula and in its central star we conclude that: i) abundances derived from CELs are, in general, lower to those found in stars for the same element; ii) considering moderate temperature fluctuations, similar to what found in the Orion nebula ($t^2 = 0.022$), and dust depletion for O, we would reconcile the abundances in the nebula and the central star for O and N. For S, the results are somewhat puzzling and points to different conclusions depending on the atomic dataset adopted for computing the ionic abundances.

As a future step, this type of study should be extended to other elements and H II regions with the aim of looking for systematic effects in the nebular/stellar abundances. Multiwavelength nebular studies taking into account aperture effects, and/or a new set of theoretical ICFs from a complete grid of H II region photoionization models, as well as multielement abundance studies from a large number of massive stars in the same star forming region would minimize uncertainties and probably would shed some light on this still poorly explored topic.

Acknowledgements. This work received financial support from the Spanish Ministerio de Educación y Ciencia (MEC) under project AYA2011-22614. JGR and SSD acknowledge support from Severo Ochoa excellence program (SEV-2011-0187) postdoctoral fellowships. We thank the anonymous referee for his/her suggestions.

References

Aller, L. H., Appenzeller, I., Baschek, B., et al. 1982, Landolt-Bornstein: Group 6: Astronomy,
 Bresolin, F., Gieren, W., Kudritzki, R.-P., et al. 2009, ApJ, 700, 309
 Brott, I., de Mink, S. E., Cantiello, M., et al. 2011, A&A, 530, A115
 Carigi, L., Peimbert, M., Esteban, C., & García-Rojas, J. 2005, ApJ, 623, 213
 Chiappini, C., Romano, D., & Matteucci, F. 2003, MNRAS, 339, 63
 Daflon, S., Cunha, K., de la Reza, R., Holtzman, J., & Chiappini, C. 2009, AJ, 138, 1577
 Delgado-Inglada, G., Morisset, C., & Stasińska, G. 2014, MNRAS, in press, arXiv:1402.4852
 Esteban, C., Bresolin, F., Peimbert, M., et al. 2009, ApJ, 700, 654
 Esteban, C., Carigi, L., Copetti, M. V. F., et al. 2013, MNRAS, 433, 382
 Esteban, C., García-Rojas, J., Carigi, L., et al. 2014, MNRAS, 443, 624
 Esteban, C., García-Rojas, J., Peimbert, M., et al. 2005, ApJ, 618, L95
 Esteban, C., Peimbert, M., García-Rojas, J., et al. 2004, MNRAS, 355, 229
 Esteban, C., Peimbert, M., Torres-Peimbert, S., & Escalante, V. 1998, MNRAS, 295, 401
 Esteban, C., Peimbert, M., Torres-Peimbert, S., & Rodríguez, M. 2002, ApJ, 581, 241
 Ferland, G. J. 1999, PASP, 111, 1524
 Gail, H.-P. & Sedlmayr, E. 1986, A&A, 166, 225
 Galavis, M. E., Mendoza, C., & Zeppen, C. J. 1995, A&AS, 111, 347
 Galavis, M. E., Mendoza, C., & Zeppen, C. J. 1997, A&AS, 123, 159
 García-Rojas, J. & Esteban, C. 2007, ApJ, 670, 457
 Harvey, P. M., Huard, T. L., Jørgensen, J. K., et al. 2008, ApJ, 680, 495
 Henry, R. B. C., Edmunds, M. G., & Köppen, J. 2000, ApJ, 541, 660
 Herbig, G. H. & Dahm, S. E. 2002, AJ, 123, 304
 Herrero, A., Kudritzki, R. P., Vilchez, J. M., et al. 1992, A&A, 261, 209
 Hunter, I., Brott, I., Lennon, D. J., et al. 2008, ApJ, 676, L29
 Irrgang, A., Przybilla, N., Heber, U., et al. 2014, A&A, in press, arXiv:1403.1122
 Jaschek, C., & Gomez, A. E. 1998, A&A, 330, 619
 Jenkins, E. B. 2009, ApJ, 700, 1299
 Jenkins, E. B. 2014, in Life Cycle of Dust in the Universe, Observations, Theory and Laboratory Experiments
 Kaufman, V. & Sugar, J. 1986, Journal of Physical and Chemical Reference Data, 15, 321
 Keenan, F. P., Hibbert, A., Ojha, P. C., & Conlonl, E. . 1993, Phys. Scr., 48, 129
 López-Sánchez, A. R., Esteban, C., García-Rojas, J., Peimbert, M., & Rodríguez, M. 2007, ApJ, 656, 168

Luridiana, V., García-Rojas, J., Aggarwal, K., et al. 2011, Summary of the Workshop: Uncertainties in Atomic Data and How They Propagate in Chemical Abundances, arXiv1110.1873

Luridiana, V., & García-Rojas, J. 2012, in IAU Symposium, Vol. 283, eds. A. Manchado, L. Stanghellini, and D. Schönberner, 139–143

Luridiana, V., Morisset, C., & Shaw, R. A. 2012, in IAU Symposium, Vol. 283, eds. A. Manchado, L. Stanghellini, and D. Schönberner, 422–423

Luridiana, V., Simón-Díaz, S., Cerviño, M., et al. 2009, *ApJ*, 691, 1712

Mendoza, C. & Zeppen, C. J. 1982, *MNRAS*, 199, 1025

Mesa-Delgado, A., Esteban, C., García-Rojas, J., et al. 2009a, *MNRAS*, 395, 855

Mesa-Delgado, A., López-Martín, L., Esteban, C., García-Rojas, J., & Luridiana, V. 2009b, *MNRAS*, 394, 693

Mesa-Delgado, A., Núñez-Díaz, M., Esteban, C., et al. 2012, *MNRAS*, 426, 614

Morel, T., Butler, K., Aerts, C., Neiner, C., & Briquet, M. 2006, *A&A*, 457, 651

Nicholls, D. C., Dopita, M. A., & Sutherland, R. S. 2012, *ApJ*, 752, 148

Nicholls, D. C., Dopita, M. A., Sutherland, R. S., Kewley, L. J., & Palay, E. 2013, *ApJS*, 207, 21

Nieva, M.-F. & Przybilla, N. 2012, *A&A*, 539, A143

Nieva, M.-F. & Simón-Díaz, S. 2011, *A&A*, 532, A2

Peña-Guerrero, M. A., Peimbert, A., & Peimbert, M. 2012, *ApJ*, 756, L14

Peimbert, A. 2003, *ApJ*, 584, 735

Peimbert, M. 1967, *ApJ*, 150, 825

Peimbert, M. 2008, *Current Science*, 95, 1165

Peimbert, M. & Costero, R. 1969, *Boletín de los Observatorios de Tonantzintla y Tacubaya*, 5, 3

Peimbert, A., & Peimbert, M. 2013, *ApJ*, 778, 89

Peimbert, M., Peimbert, A., Esteban, C., et al. 2007, in *Revista Mexicana de Astronomía y Astrofísica*, vol. 27, Vol. 29, *Revista Mexicana de Astronomía y Astrofísica Conference Series*, ed. R. Guzmán, 72–79

Peimbert, M., Storey, P. J., & Torres-Peimbert, S. 1993, *ApJ*, 414, 626

Podobedova, L. I., Kelleher, D. E., & Wiese, W. L. 2009, *Journal of Physical and Chemical Reference Data*, 38, 171

Pradhan, A. K., Montenegro, M., Nahar, S. N., & Eissner, W. 2006, *MNRAS*, 366, L6

Puls, J., Kudritzki, R.-P., Herrero, R., et al. 1996, *A&A*, 305, 171

Puls, J., Urbaneja, M. A., Venero, R., et al. 2005, *A&A*, 435, 669

Ramsbottom, C. A., Bell, K. L., & Stafford, R. P. 1996, *Atomic Data and Nuclear Data Tables*, 63, 57

Rivero González, J. G., Puls, J., & Najarro, F. 2011, *A&A*, 536, A58

Rivero González, J. G., Puls, J., Najarro, F., & Brott, I. 2012, *A&A*, 537, A79

Santolaya-Rey, A. E., Puls, J., & Herrero, A. 1997, *A&A*, 323, 488

Simón-Díaz, S. 2010, *A&A*, 510, A22

Simón-Díaz, S., Castro, N., Herrero, A., et al. 2011a, *Journal of Physics Conference Series*, 328, 012021

Simón-Díaz, S., García-Rojas, J., Esteban, C., et al. 2011b, *A&A*, 530, A57

Simón-Díaz, S. & Herrero, A. 2014, *A&A*, 562, A135

Simón-Díaz, S. & Stasińska, G. 2011, *A&A*, 526, A48

Sofia, U. J., Cardelli, J. A., & Savage, B. D. 1994, *ApJ*, 430, 650

Sofia, U. J., & Meyer, D. M. 2001, *ApJ*, 554, L221

Stasińska, G., Tenorio-Tagle, G., Rodríguez, M., & Henney, W. J. 2007, *A&A*, 471, 193

Storey, P. J., & Hummer, D. G. 1995, *MNRAS*, 272, 41

Tayal, S. S. 2011, *ApJS*, 195, 12

Tayal, S. S. & Gupta, G. P. 1999, *ApJ*, 526, 544

Telting, J. H., Avila, G., Buchhave, L., et al. 2014, *AN*, 335, 41

Torres-Peimbert, S. & Peimbert, M. 1977, *Rev. Mexicana Astron. Astrofis.*, 2, 181

Tremonti, C. A., Heckman, T. M., Kauffmann, G., et al. 2004, *ApJ*, 613, 898

Trundle, C., Dufton, P. L., Lennon, D. J., Smartt, S. J., & Urbaneja, M. A. 2002, *A&A*, 395, 519

Tsamis, Y. G. & Péquignot, D. 2005, *MNRAS*, 364, 687

Tsamis, Y. G., Walsh, J. R., Vílchez, J. M., & Péquignot, D. 2011, *MNRAS*, 412, 1367

U, V., Urbaneja, M. A., Kudritzki, R.-P., et al. 2009, *ApJ*, 704, 1120

Wyse, A. B. 1942, *ApJ*, 95, 356

White, B. & Sofia, U. J. 2011, in *American Astronomical Society Meeting Abstracts #218*, #129.23

Zeppen, C. J. 1982, *MNRAS*, 198, 111

ula is located. The proposed values ranges from 460 to 1400 pc. We refer the reader to Harvey et al. (2008) for a complete compilation of published distance estimates previous to 2008, and a detailed discussion of the various considered methodologies and their reliability.

In this paper, we were mainly interested in the quantitative spectroscopic analysis of BD+46 3474 to determine its photospheric chemical composition and compare the derived abundances with those resulting from the study of the Cocoon nebula spectrum. However, as a plus, we can also reevaluate the issue of the distance to this star and its associated H II region using state-of-the-art information. Below, we describe the methodology we have followed and our proposed value.

Table 3 summarized the spectroscopic parameters (T_{eff} and $\log g$, among others) resulting from the FASTWIND analysis, as well as some photometric information that we use for the evaluation of the distance (namely, the V magnitude and the B-V color). From the comparison of intrinsic $(B-V)_0$ color predicted by a FASTWIND model with the indicated T_{eff} and $\log g$ and the observed value, we obtained the value of the extinction parameter in the V band. We hence determined M_V , R , $\log L$, and M_{sp} (spectroscopic mass) assuming several values of the distance. The absolute visual magnitude was computed by means of

$$M_V = V - 5 \log d + 5 - A_V \quad (\text{A.1})$$

and the stellar radius, luminosity, and spectroscopic mass was derived by means of the strategy indicated in Herrero et al. (1992). Last, we located the star in the HR diagram and computed the evolutionary mass by comparing with the evolutionary tracks by Brott et al. (2011).

Table A.1 and Figure A.1 summarizes the results from this exercise. From inspection of Figure A.1 it becomes clear that any distance below 720 pc is not possible since the star would be located below the zero-age main sequence (ZAMS) line. We have selected four distances above that value. The largest one (1.2 Kpc) is the value proposed by Herbig & Dahm (2002) based on the spectroscopic distances to the late-B stars and two different main-sequence calibrations: Jaschek & Gomez (1998) absolute magnitudes for B dwarf standards, and the Schmidt-Kaler ZAMS Aller et al. (1982). The other values are our suggested distance (800 pc), the value proposed by Harvey et al. (2008), and an intermediate value.

As illustrated in Table A.1 and Figure A.1 the determined spectroscopic mass, evolutionary mass and age are a function of the assumed distance. We can clearly discard the 1200 pc (and even the 950 pc) solutions since these distances result in a very bad agreement between the spectroscopic and evolutionary masses and a too evolved star (≥ 4 Myr). Note that given the high number of accreting pre-MS stars, we expect the age of the IC 5146 cluster to be less than a few Myr (Herbig & Dahm, 2002; Harvey et al., 2008). We hence use the $M_{\text{sp}}=M_{\text{ev}}$ criterium to propose 800 ± 80 pc as the distance to BD+46 3474.

Appendix A: On the distance to the Cocoon nebula as determined from BD +46 3474

There have been several independent determinations of the distance to the IC 5146 star-forming region, where the Cocoon neb-

Table A.1. Computed values of absolute visual magnitude, stellar radius, luminosity, spectroscopic mass, evolutionary mass and age for different assumed distances to BD+46 3474 (see Sect. A for explanations). We indicate in bold our proposed distance.

d (pc)	M_v	R (R_\odot)	$\log(L/L_\odot)$	M_{sp} (M_\odot)	M_{ev} (M_\odot)	Age (Myr)
720	-2.8	4.7	4.23	13	14–15	ZAMS
800	-3.0	5.2	4.31	15	~15	2
850	-3.2	5.5	4.37	18	15–16	3
950	-3.4	6.2	4.47	22	~16	4
1200	-3.9	7.8	4.68	35	~18	6

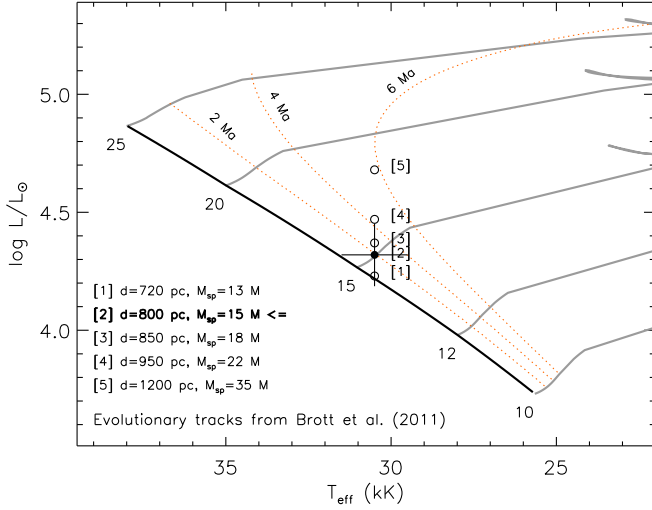


Fig. A.1. Location of BD+46 3474 in the HR diagram for different values of assumed distance (see also Table A.1. Evolutionary tracks and isochrones from Brott et al. (2011). The corresponding spectroscopic masses are also indicated.